Novel Zinc β-Diketonates with Donor–Acceptor Ligands: Synthesis and Comprehensive Structural, Thermal, and Photophysical Characterization

Ahmad Daher , Manjiri Choudhari , Thomas Roland , Vincent De Waele , Stephane Daniele *

Posted Date: 30 September 2025

doi: 10.20944/preprints202509.2570.v1

Keywords: zinc β-diketonates; homoleptic and heteroleptic complexes; structural characterization; thermal analysis; femtosecond transient absorptio

Article

Novel Zinc β-Diketonates with Donor–Acceptor Ligands: Synthesis and Comprehensive Structural, Thermal, and Photophysical Characterization

Ahmad Daher [1], Manjiri Choudhari [2], Thomas Roland [2], Vincent De Waele [2] and Stéphane Daniele [1,*]

[1] CP2M-ESPCE Lyon, CNRS-UMR 5128, University Lyon 1, F-69100 Villeurbanne, France;

[2] LASIRe, CNRS-UMR 8516, University of Lille, F-59000 Lille, France;

* Correspondence: stephane.daniele@univ-lyon1.fr

Abstract

We report the synthesis, structural characterization, and ultrafast photophysical investigation of a novel series of homoleptic and heteroleptic Zn(II) β-diketonates derived from donor–acceptor ligands. Single-crystal X-ray diffraction revealed that all complexes adopt monomeric octahedral geometries, with ancillary nitrogen-based ligands inducing variable distortions. UV–Vis absorption and femtosecond transient absorption spectroscopy established that the chelated β-diketonate ring constitutes the primary optically active chromophore, while Zn coordination markedly alters excited-state dynamics. In contrast to the free ligand, which undergoes rapid internal conversion, Zn binding stabilizes the triplet state, generating a long-lived and chemically reactive species. Thermal and mass spectrometric analyses confirmed their stability and decomposition pathways, supporting their potential use as precursors for laser-induced three-dimensional ZnO growth. Such features underline the relevance of these complexes in photonic and electronic applications where controlled nanostructure development is required. Overall, these findings provide fundamental insights into structure–photophysics relationships in Zn β-diketonates. They demonstrate how tailored ligand environments can be exploited to tune excited-state properties, offering a rational framework for the design of functional precursors suitable for nonlinear photolysis and advanced nanomaterial synthesis.

Keywords: zinc β-diketonates; homoleptic and heteroleptic complexes; structural characterization; thermal analysis; femtosecond transient absorption

1. Introduction

β-Diketonate ligands ($R^1COCHR^3COR^2$) are among the most versatile and widely exploited classes of precursors for metal–organic chemical vapor deposition (MOCVD) of thin films. Their tunable volatility, coordination flexibility, and favorable decomposition behavior make them especially suited for gas-phase delivery of metal centers. For example, fluorinated β-diketonate complexes $M(tfac)_2(TMEDA)$ (M = Fe, Ni, Cu, Zn) have recently been demonstrated as effective MOCVD precursors to deposit both metal and metal oxide films, with controlled film quality (i.e., well-oriented ZnO thin films) and composition, thereby highlighting the critical role of ligand design in optimizing volatility and film quality [1]. Previous results from our group have highlighted how γ-substitution (R^3 nature) can be exploited to tune the stability and reactivity (degradation mechanism) of titanium β-diketonate precursors, paving the way for the rational design of improved molecules for TiO_2 thin-film deposition [2].

ZnO is an attractive target material due to its wide bandgap, biocompatibility, piezoelectric properties, and relevance in microelectromechanical systems (MEMS), actuators, sensors, photonics, and solar cells. β-Diketonate ligands ($R^1COCHR^3COR^2$) are particularly suitable for this purpose

 doi:10.20944/preprints202509.2570.v1

because they act as chelating ligands that promote electron delocalization when coordinated to metal ions. By forming donor–π–acceptor complexes with Zn^{2+} ions, these ligands facilitate low-energy ligand-to-metal charge transfer (LMCT) [3], enhancing multiphoton absorption and enabling controlled laser-induced material growth. Structural versatility can be achieved by modifying the R^1, R^2, and R^3 substituents, providing additional control over precursor properties.

The development of next-generation micro- and nanotechnologies for microelectronic, photonic, and MEMS/NEMS components requires fabrication processes that operate in three dimensions, are flexible, fast, and parallel, and scalable, while minimizing the use of environmentally costly elements [4–8]. Conventional micro synthetic techniques, however, are largely limited to 2.5D processing and cannot achieve true 3D structuring at the sub-micrometer scale [9–12]. High-throughput additive manufacturing is often restricted either to feature sizes of tens of micrometers or to organic polymers, limiting its applicability for functional inorganic materials [13–15].

Ultrashort laser excitation induces complex coherent superpositions of excited states that evolve on femtosecond timescales through internal conversion or direct relaxation to the ground state, often accompanied by excess vibrational energy. These ultrafast processes depend on the metal center, ligand type, and excitation conditions, and can be tuned by adjusting the coordination environment to control solubility, electronic and optical properties, and decomposition pathways. Chemical deposition using femtosecond laser pulses offers a promising approach to achieve precise 3D growth of inorganic materials [16]. This approach requires the design of molecular precursors that efficiently absorb multiphotonic excitation and undergo controlled ligand degradation. Nonlinear photolysis enables progressive growth of inorganic materials at sub-micrometer scales, providing a flexible route for 3D fabrication [17]. The main challenges remain: (i) designing precursor molecules with high multiphoton absorption and efficient ligand decomposition, and (ii) understanding the ultrafast photo physics and photochemistry underlying the reactions [9–13].

To date, such ligand architectures have not been systematically explored with ultrafast spectroscopic techniques. In this study, we report the synthesis and full characterization of a novel series of homoleptic and heteroleptic β-diketonate Zn(II) complexes. Their structural, thermal, and electronic properties were examined by X-ray diffraction, NMR, UV–Vis spectroscopy, mass spectrometry, and thermal analysis. In addition, femtosecond spectroscopy was employed to probe their excited-state dynamics, providing new insights into the photophysical behaviour of these complexes. We further investigate the influence of different ancillary ligands on stability, optical properties, and excited-state relaxation pathways. This comprehensive study establishes important structure–property relationships for Zn(II) β-diketonates, laying the groundwork for their future application as ZnO precursors and functional materials.

2. Results and Discussion

2.1. Spectroscopic Characterizations

The zinc β-diketonate complexes were synthesized via a Brønsted acid–base reaction between the enolic form of the ligand **L^1H** and $ZnEt_2$ in a 2:1 molar ratio, producing ethane as the only byproduct. The reaction conditions determined the formation of either nonhydrated homoleptic complexes or heteroleptic analogues in moderate to excellent yields (50–90%) Scheme 1. Exposing the reaction mixture to air yielded the hydrated product **2**, while addition of nitrogen-based Lewis bases (TMEDA, bipyridine, *o*-phen) led to the formation of complexes **3–5**. Substitution of water molecules by Lewis bases is thermodynamically favourable, primarily due to entropic effects.

 doi:10.20944/preprints202509.2570.v1

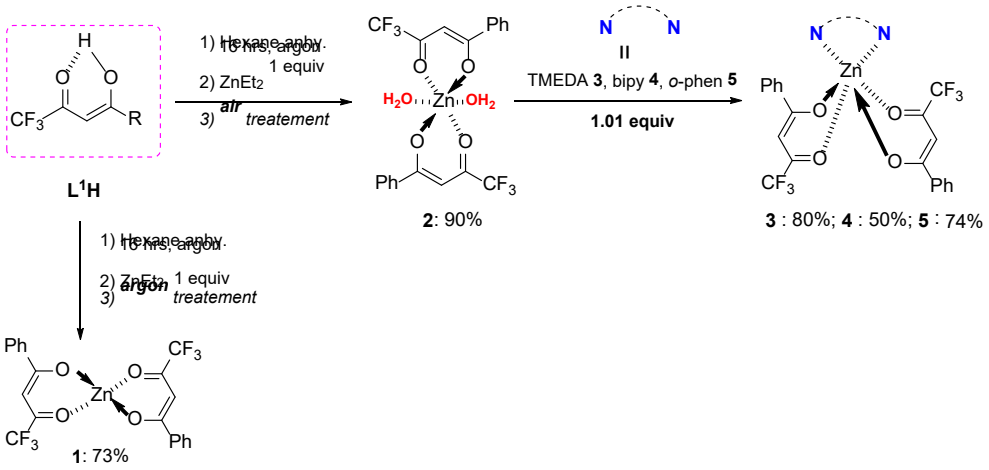

Scheme 1. Synthesis of the zinc complexes **1**-**5** starting from ligands **L^{1}H.**

All complexes exhibit solubility in polar organic solvents. Characterization by ^{1}H and ^{19}F spectroscopy NMR (See supporting information for spectra) confirms coordination between the β-diketonate ligands and the Lewis bases for the heteroleptic complexes; no uncoordinated ligands were detected. Interestingly, coordination induces only minor chemical shift changes in the ^{1}H NMR spectra.

FT-IR spectra further support complex formation (See supporting information for individual spectra). **L^{1}H** exhibits a C=O stretching band at 1600 cm^{-1}, indicative of a predominant ketone form. In complex **2**, coordination leads to enolization, with the appearance of a C–O stretching band at 1311 cm^{-1} and a broad O–H band at 3363 cm^{-1} corresponding to hydrogen-bonded water. In complexes **3–5**, the O–H band disappears as water is replaced by Lewis bases. C=C stretching bands remain relatively unchanged across all complexes (1573–1577 cm^{-1}), while the C–O band in **5** shifts to 1286 cm^{-1}, suggesting stronger π-backbonding interactions with *o*-phenanthroline.

2.2. Single-Crystal X-Ray Characterizations of the Zinc Complexes

The structures of complexes **2–5** were determined by slow evaporation of saturated acetonitrile solutions Figure 1. Crystallographic data are summarized in

Table 1, and selected bond lengths and angles in Table 2.

All complexes are monomeric, with zinc atoms in a hexa-coordinated octahedral geometry [18]. Complex **2** exhibits a regular octahedral structure with two β-diketonate ligands in a trans configuration. In contrast, heteroleptic complexes **3–5** adopt cis configurations due to the chelating nature of the Lewis bases, resulting in distorted octahedral geometries. The extent of distortion correlates with ligand rigidity: TMEDA in **3** produces minimal distortion, while bipy and *o*-phen in **4** and **5** induce larger deviations from ideal bond angles.

 doi:10.20944/preprints202509.2570.v1

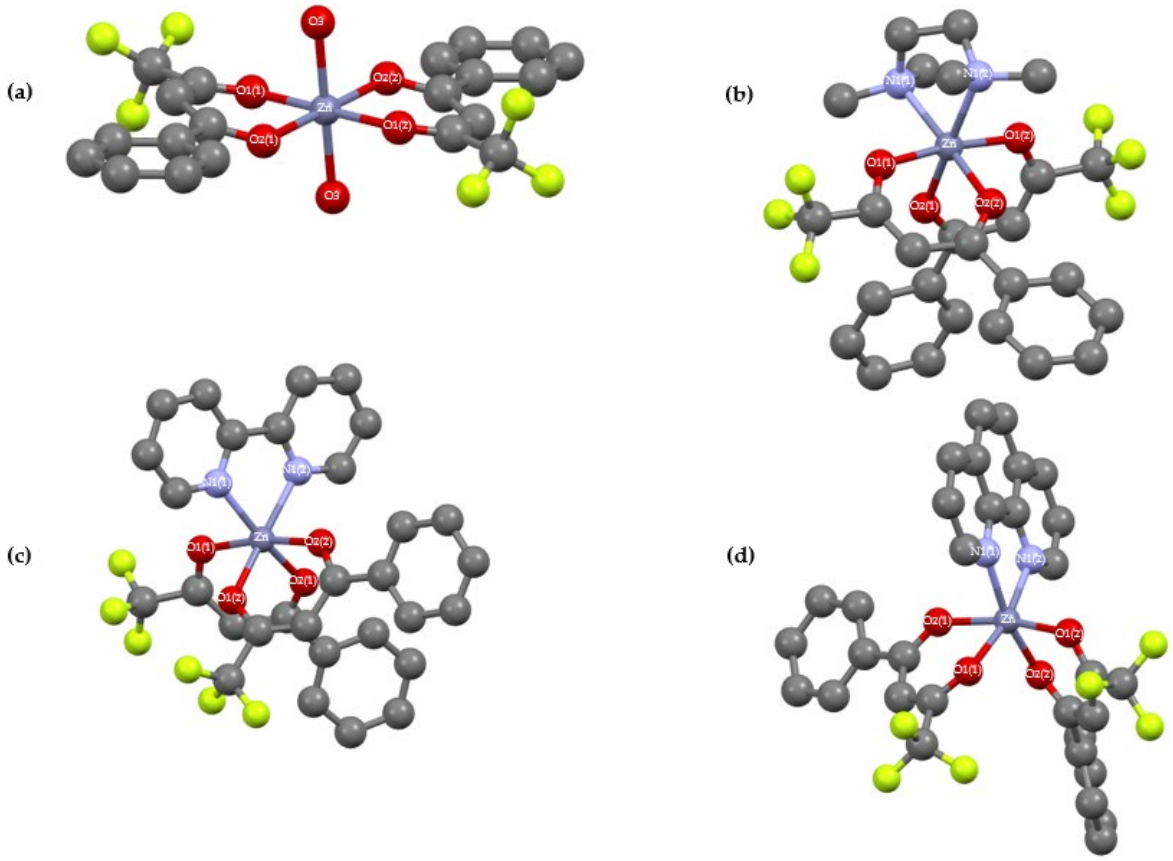

Figure 1. (**a-d**) depict the crystal structures of the four complexes, illustrating the geometric differences between hydrated and heteroleptic species. (a) Crystal structure of $[Zn(L^1)_2(H_2O)_2]$ **(2); (b)** Crystal structure of $[Zn(L^1)_2(TMEDA)]$ **(3); (c)** Crystal structure of $[Zn(L^1)_2(bipy)]$ **(4); (d)** Crystal structure of $[Zn(L^1)_2(o\text{-}phen)]$ **(5).**

Table 1. Crystallographic data of complexes $[Zn(L^1)_2(H_2O)_2]$ **(2),** $[Zn(L^1)_2(TMEDA)]$ **(3),** $[Zn(L^1)_2(bipy)]$ **(4)** and **[**$Zn(L^1)_2(o\text{-}phen)$**]** **(5).**

Complex	**2**	**3**	**4**	**5**
Formula	$C_{20}H_{16}O_6F_6Zn$	$C_{26}H_{28}N_2O_4F_6Zn$	$C_{30}H_{20}N_2O_4F_6Zn$	$C_{32}H_{20}N_2O_4F_6Zn$
M. W.	531.70	611.87	651.85	675.87
C. S.	Triclinic	Orthohombic	Triclinic	Triclinic
S. G.	*P*-1	$P2_12_12$	*P*-1	*P*-1
a (Å)	4.80150(10)	8.53980(10)	8.5766(2)	8.81410(10)
b (Å)	9.5125(2)	18.7656(2)	10.8852(2)	10.8811(2)
c (Å)	11.5291(2)	17.20870(10)	15.7069(3)	15.5729(3)
α (°)	75.925(2)	90	90.703(2)	94.330(2)
β (°)	78.557(2)	90	92.936(2)	94.6610(10)
γ (°)	80.2440(10)	90	106.838(2)	104.339(2)
V (Å^3)	496.536(18)	2757.77(5)	1401.09(5)	1435.15(4)
Z	1	4	4	2
***p* (g.cm^{-3})**	1.778	1.474	1.545	1.564
***μ* (mm^{-1})**	1.330	0.965	0.956	1.913
***F*(000)**	268	1256	660	684
***Size* (mm^3)**	0.28×0.14×0.02	0.40×0.12×0.11	0.30×0.26×0.20	0.11×0.07×0.02
***θ range* (°)**	2.565 to 30.286	2.367 to 30.946	2.317 to 30.402	2.861 to 77.775
R. C.	21817	184638	62557	38401
I. R.	2677	8024	7525	5687

 doi:10.20944/preprints202509.2570.v1

Goodness	1.086	1.048	1.076	1.041
R [I>2α(I)]	2483	7307	6597	5220
wR2	0.0608	0.0716	0.0871	0.1083

Table 2. Selected bond lengths and angles of complexes $[Zn(L^1)_2(H_2O)_2]$ **(2),** $[Zn(L^1)_2(TMEDA)]$ **(3),** $[Zn(L^1)_2(bipy)]$ **(4)** and **[**$Zn(L^1)_2(o\text{-phen})$**] (5).**

Å	2	3	4	5
Zn1-O1(1)	2.053	2.07	2.106	2.071
Zn1-O1(2)	2.053	2.07	2.058	2.071
Zn1-O2(1)	2.095	2.091	2.069	2.133
Zn1-O2(2)	2.095	2.091	2.125	2.067
Zn1-O3(1)	2.120	-	-	-
Zn1-O3(2)	2.120	-	-	-
Zn1-N1(1)	-	2.181	2.119	2.137
Zn1-N1(2)	-	2.181	2.123	2.148
º	**2**	**3**	**4**	**5**
O1(1)-Zn1-O2(1)	87.04	85.56	84.62	84.45
O1(2)-Zn1-O2(1)	92.96	89.66	170.02	168.38
O1(1)-Zn1-O2(2)	92.96	89.66	95.85	97.25
O1(2)-Zn1-O2(2)	87.04	85.66	85.77	86.59
O1(1)-Zn1-O3(1)	90.38	-	-	-
O1(2)-Zn1-O3(1)	89.62	-	-	-
O1(1)-Zn1-O3(2)	89.62	-	-	-
O1(2)-Zn1-O3(2)	90.38	-	-	-
O2(1)-Zn1-O3(1)	88.02	-	-	-
O2(2)-Zn1-O3(1)	91.98	-	-	-
O2(1)-Zn1-O3(2)	91.98	-	-	-
O2(2)-Zn1-O3(2)	88.02	-	-	-
O1(1)-Zn1-O1(2)	180	173.11	86.16	84.83
O2(1)-Zn1-O2(2)	180	92.25	91.38	90.33
O1(1)-Zn1-N1(1)	-	95.56	96.01	95.24
O1(2)-Zn1-N1(1)	-	87.80	87.55	91.06
O1(1)-Zn1-N1(2)	-	87.80	166.40	167.17
O1(2)-Zn1-N1(2)	-	95.56	105.06	105.88
O2(1)-Zn1-N1(1)	-	92.55	97.20	94.37
O2(2)-Zn1-N1(1)	-	172.50	165.96	167.02
O2(1)-Zn1-N2(1)	-	172.50	84.61	85.34
O2(2)-Zn1-N2(2)	-	92.55	92.69	95.54
N1(1)-Zn1-N1(2)	-	82.86	77.15	77.82

2.3. Thermal Analysis

Thermogravimetric analysis (TGA) was performed from room temperature to 600 °C to investigate thermal stability and volatility Figure 2. **L^1H** displays moderate volatility with an onset of 120 °C, attributed to the π-stacking interactions of the phenyl groups. Coordination with zinc enhances thermal stability, with all complexes showing weight loss above 250 °C. Complex **2** exhibits an initial 6% mass loss at 120 °C, corresponding to water release. Complex **3**, which is anhydrous, shows volatility comparable to the hydrated **2** after its dehydration. The Lewis base nature has limited effect on thermal stability, except for *o*-phen in complex **5**, which increases the decomposition temperature by ~50 °C and produces a higher residual mass (66%) compared to bipy (46%) and TMEDA (38%).

 doi:10.20944/preprints202509.2570.v1

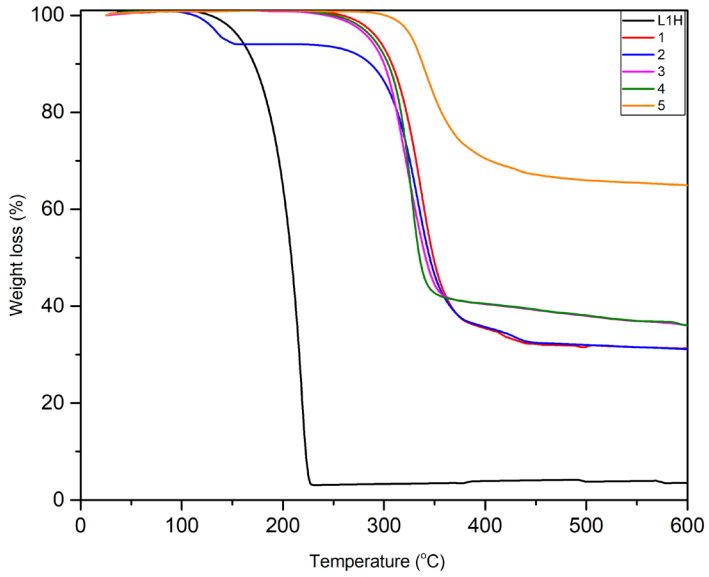

Figure 2. TGA curves of **L^1H** and complexes $[Zn(L^1)_2]_m$ **(1),** $[Zn(L^1)_2(H_2O)_2]$ **(2),** $[Zn(L^1)_2(TMEDA)]$ **(3),** $[Zn(L^1)_2(bipy)]$ **(4)** and **[**$Zn(L^1)_2(o\text{-}phen)]$ **(5).**

For complexes **1–3**, the final residues after TGA at 600 °C can be attributed mainly to ZnO and ZnF_2, as the experimental values are close to the sum of their theoretical residues in addition to small amounts of char residues which is common in such TGA analyses [19]. ZnF_2 is known to form from zinc β-diketonate complexes (e.g., bis(2,2,6,6-tetramethyl-3,5-heptanedionato)zinc) in the presence of a fluorine source. In contrast, for complexes **4** and **5**, the addition of aromatic ligands such as bipy and o-phen leads to higher experimental residues [19]. This indicates that the final residue in these cases includes not only ZnO and ZnF_2 but also residual carbon from the decomposition of the aromatic ligands Table 3.

Table 3. Expected vs experimental residual yields for ZnO and ZnF_2.

Complex	Theoretical % of residues for ZnO	Theoretical % of residues for ZnF_2	Experimental % residues at 600 °C
1	**16**	21	32
2	**15**	17	32
3	**13**	28	38
4	**12**	23	46
5	**12**	21	66

2.4. ESI/FAB Mass Spectrometry

ESI/FAB analysis of all complexes in ethanol revealed the parent $[M + Na]^+$ ions and characteristic fragmentation patterns Scheme 2 (For more details check the mass spectra in the supporting information). The base peak corresponds to the loss of one β-diketonate ligand. In heteroleptic complexes **3–5**, subsequent loss of the Lewis base is observed, supporting the proposed coordination. Protonated free Lewis bases were also detected.

 doi:10.20944/preprints202509.2570.v1

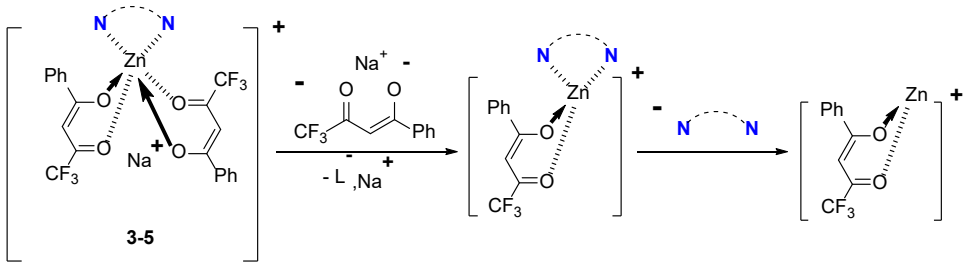

Scheme 2. The proposed fragmentation of the heteroleptic complexes **3-5.**

2.5. Femtosecond Transient Absorption Spectroscopy (TAS)

The ground-state electronic transitions of complexes **2–5** were studied alongside **L¹H** using steady-state absorption spectroscopy. **L¹H** exhibits a strong absorption band at 330 nm and a secondary peak at 260 nm, consistent with related dibenzoylmethane derivatives [20]. The intense band at 330 nm is assigned to a $\pi \rightarrow \pi^*$ (S_0-S_n) transition associated with the chelated ring of **L¹H**.

In Figure 3, the absorption band of s **2-5** is around 330 nm is retained but exhibits a slight blue shift of approximately 8 nm. Additionally, in complexes **4** and **5**, absorption bands corresponding to the bipy, 265 nm and *o*-phen, 280–320 nm moieties are observed. The UV–Vis spectra of the complexes are dominated by the absorption of **L¹H**, which has a $\pi \rightarrow \pi^*$ character, while contributions from the ancillary ligands are observed only below 300 nm.

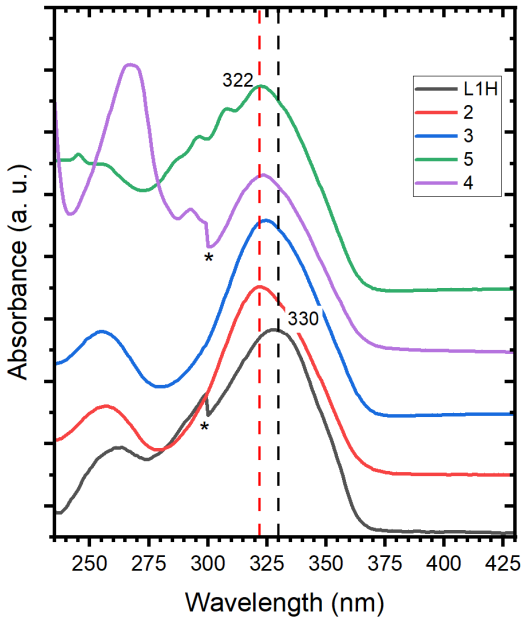

Figure 3. UV-vis absorption spectra of compounds **L¹H** and complexes, $[Zn(L^1)_2(H_2O)_2]$ **(2),** $[Zn(L^1)_2(TMEDA)]$ **(3),** $[Zn(L^1)_2(bipy)]$ **(4)** and **[**$Zn(L^1)_2$(o-phen)] **(5)** in ethanol (10^{-5} M). The spectra have been vertically shifted for clarity. The stars mark an artefact from the spectrometer.

UV–Vis transient absorption experiments were conducted to characterize the excited states formed upon photoexcitation of the compounds, with particular focus on assessing the influence of the ancillary ligands. All transient spectra were recorded in ethanol upon photoexcitation at 320 nm, in resonance with the optically active $\pi \rightarrow \pi^*$ transition. The results obtained for the compound **L¹H** are shown in Figure 4. The spectral evolution can be described as a sequence of four steps. In Figure 4a, between 0 and 140 fs, we observe the development of an excited-state absorption (ESA) band

 doi:10.20944/preprints202509.2570.v1

peaking at 375 nm, along with a stimulated emission (SE) feature reaching its maximum amplitude at 425 nm. The SE band indicates an optically allowed transition, suggesting that the transient species observed at 140 fs corresponds to the π→π* state. As shown in Figure 4b, this π→π* state evolves into a new transient species within less than 1 ps, characterized by reduced ESA intensity below 400 nm and the appearance of a new ESA band with a maximum at 525 nm. Concomitantly, the SE band of the π→π* state disappears, indicating its conversion to a non-emitting state. A negative feature below 370 nm is also observed, which can be assigned to the ground-state bleach (GSB). The ESA of this transient state is significantly less intense than that of the π→π* state. After 1 ps, spectral changes become less pronounced. Between 1 and 10 ps, the evolution is characterized by a decay of the ESA below 400 nm accompanied by partial recovery of the GSB, a behavior typical of vibrational cooling of a hot ground state. Finally, the weak ESA gradually vanishes over several hundred picoseconds.

The transient absorption spectra have been investigated for the compounds **2-5** under similar conditions as for **L^{1}H**. The results are qualitatively similar for the four compounds (Figure 5 and SI-figures **12-14**). The TAS recorded for the complexes are significantly different from those of **L^{1}H**. In Figure 5a) we can recognize the formation of the ππ* excited by its ESA at 370 nm and the SE contribution around 425 nm. However, compared to **L^{1}H**, the TAS exhibits a new strong ESA contribution with a maximum of absorption around 550-600 nm. Within less than 1 ps, the ESA decreases together with the SE, an isobestic point is observed at 400 nm, and there is a small decrease of the red-tail of the ESA at 575 nm. This corresponds to internal conversion from the ππ* to a less-emitting, excited state Figure 5b. The second transient species is converted into a third (Figure 5c) characterized by an ESA band with a maximum of absorption at 625 nm. Finally, the spectrum of this last species does not evolve on the nanosecond time, indicating the formation of a long-living transient (ns-μs timescale or longer). Very similar transient spectra and kinetic evolution were obtained for the compound **2-5** (see SI), with no significant change in the kinetics.

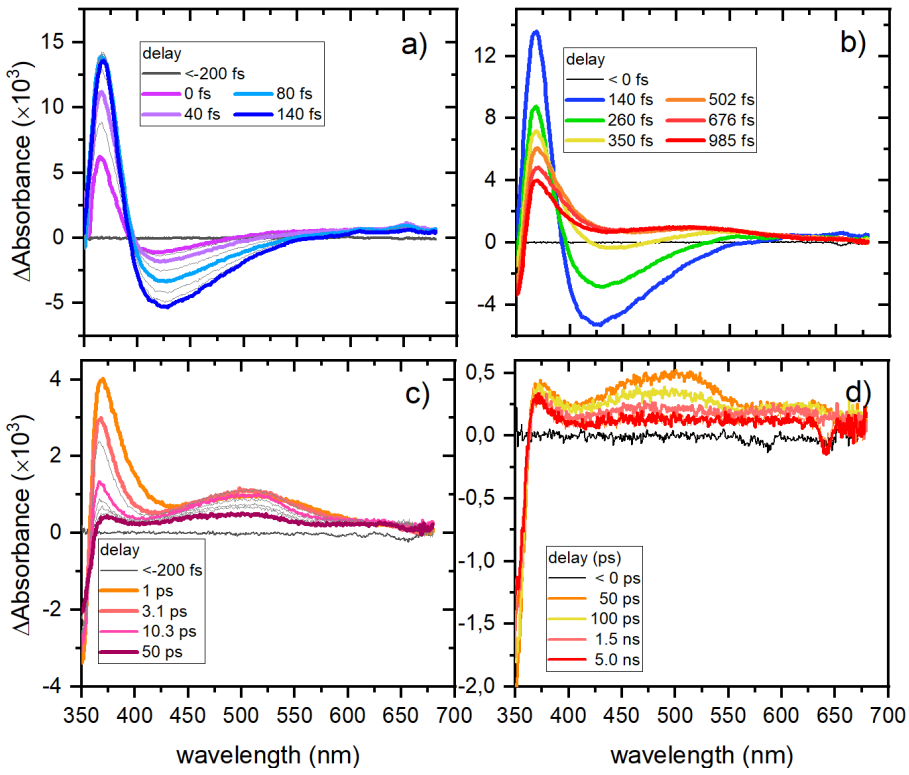

Figure 4. Transient absorption spectra of compounds **L^{1}H** recorded in ethanol with a pump excitation λ_{pump} = 320 nm.

 doi:10.20944/preprints202509.2570.v1

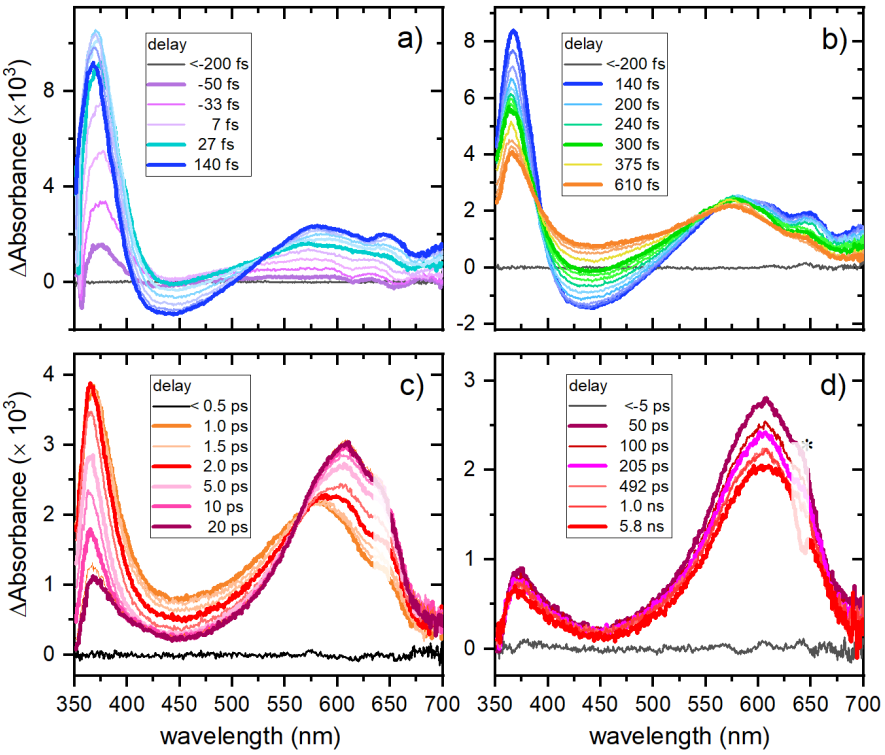

Figure 5. Transient absorption spectra of compounds $[Zn(L^1)_2(H_2O)_2]$ **(2)** recorded in ethanol with a pump excitation λ_{pump} = 320 nm.

3. Discussion

In this work, we synthesized a novel family of Zn β-diketonate complexes, and report their photophysical properties for the first time with respect to potential laser deposition applications. Our study focuses on the characterization of transient species; their specific photoreactivity will be detailed in a forthcoming manuscript.

From the UV–Vis absorption spectra, it is evident that the lowest optically allowed electronic transition is the same for **L¹H** and complexes **1–5**, irrespective of the nature of the ancillary ligand. This demonstrates that the chelated ring constitutes the main chromophore responsible for the optical transition, and that the first populated excited state upon absorption of a UV photon around 320 nm corresponds to the π→π* state of the **L¹H** ligand. The ultrafast photodynamics observed for **L¹H** are in good agreement with previous experimental and theoretical studies on β-diketones [21]. The bright π→π* state corresponds to the S_2 state, which undergoes internal conversion to the S_1 n→π* state and to a hot S_0 ground state in less than 1 ps. Internal conversion to the ground state constitutes the main relaxation pathway, while the small absorption band observed on the picosecond timescale arises from a minor contribution of intersystem crossing (ISC) to the triplet state and the formation of a trans isomer. After several hundred picoseconds, the ground state is fully recovered.

Chelation of Zn significantly modifies the photodynamics of the **L¹H** moiety, even though the first populated state remains a π→π* state. The most notable effect of chelation is the hindrance of ultrafast internal conversion to the ground state due to the increased structural rigidity, resulting in a sequence of three observable transient species. Upon light absorption, the S_2 π→π* state is first populated, followed by ultrafast internal conversion to the S_1 state, which retains n→π* character but exhibits a stronger and red-shifted ESA band compared to **L¹H**. This new ESA feature indicates that the chelated ring remains intact and may also involve a ligand-to-metal charge transfer contribution. The S_1 state subsequently evolves into a new state, assigned to the triplet state of the β-diketonate ligand.

 doi:10.20944/preprints202509.2570.v1

Theoretical calculations are needed to clarify the exact contributions of the n→π*, charge-transfer, or ligand-field character, but our data demonstrate that the ancillary ligands are not significantly involved. While for **L^{1}H** the main photophysical pathway is ultrafast internal conversion to the ground state, in complexes **1–5** the majority of the absorbed energy remains trapped in the excited triplet state. This is a remarkable property, as the triplet state of the ketones is chemically active and can, for example, undergo hydrogen abstraction from the solvent leading to a potential pathway for complex destabilization. The photo reactivity of these compounds will be discussed in a separate study.

Overall, these results highlight the key role of Zn chelation in modulating the photo dynamics of β-diketonates, providing longer-lived excited states that may be advantageous for applications in laser deposition. The combination of ultrafast spectroscopy and preliminary computational analysis offers a coherent picture of the transient species involved and sets the stage for further studies aimed at understanding their photochemical behaviour and potential reactivity pathways.

4. Materials and Methods

The FT-infrared spectra (FT-IR) of the ligand and complexes were recorded using a Nicolet iS50 FT-IR spectrometer. UV-visible absorbance measurements were performed using Thermo Scientific Evolution 220 dual-beam spectrophotometer at a scan rate 1 nm / sec. ^{1}H and ^{19}F NMR spectra were acquired on a Bruker SampleXpress 300 MHz spectrometer (s = singlet, d = doublet, t = triplet, m = multiplet). ESI/FAB mass spectra were recorded using an Impact II mass spectrometer by electrospray ionization (ESI); FAB conditions are indicated in the Supporting Information. Thermal behavior was analyzed using a METTLER TOLEDO TGA 2 Star System under a nitrogen atmosphere at a scan rate of 5 K min^{-1}. Femtosecond transient absorption measurements have been carried out using the set-up described in [22]. Briefly, the system consists of a 5 W Astrella laser delivering 35 fs pulses used to seed an OPA and a Helios UV–vis transient absorption spectrometer. All the measurements were performed in solution using a 1 mm flowing cell.

Single crystal X-ray diffraction data of complexes **2-5** were measured using ω scans with Mo Kα radiation at 100 K. The diffraction pattern was indexed and the total number of runs and images was based on the strategy calculation from the program CrysAlisPro system (CCD 43.125a 64-bit (release 04-06-2024)). The maximum resolution that was achieved was Θ = 30.615° (0.70 Å). The unit cell was refined using CrysAlisPro 1.171.43.124a (Rigaku OD, 2024) on 20645 reflections, 64% of the observed reflections. Data reduction, scaling and absorption corrections were performed using CrysAlisPro (Rigaku Oxford Diffraction). A multi-scan absorption correction (SCALE3 ABSPACK) was applied. The dataset is 100% complete to 30.615° in θ. The absorption coefficient (μ) is 0.945 mm^{-1} at λ = 0.71073 Å. Minimum and maximum transmissions are 0.768 and 1.000. Data were collected at 100 K. Cell parameters and orientation matrices were determined from 36 frames of 2 D diffraction images. The data were corrected for Lorentz and polarization effects.

$ZnEt_2$ (CAS no: 557-20-0) in toluene solution (2 M) and 4,4,4-trifluoro-1-phenylbutane-1,3-dione (**L^{1}H)** (CAS no: 720-94-5) were purchased from Thermo Fisher Scientific and Merck-Sigma Aldrich companies, respectively and used without further purification. Nitrogen-based Lewis bases : N,N,N',N'-Tetramethylethylenediamine (TMEDA, CAS no: 612-00-3), 2,2' bipyridine (bipy, CAS no: 366-18-7) and 1,10-phenanthroline monohydrate (*o*-phen, CAS no: 66-71-7) were purchased from Merck-Sigma Aldrich and Alfa Aesar companies, respectively, and used without any further purification.

L^{1}H : $C_{10}H_7O_2F_3$. 216 g.mol^{-1}. ^{1}H NMR (MHz, CD_2Cl_2, δ ppm) : 7.97 (2H, d, J = 7.23 Hz, HC_{ar}) ; 7.66 (1H, t, J = 7.38 H, HC_{ar}) ; 7.53 (2H, t, J = 7.7 Hz, HC_{ar}) ; 6.62 (1H, s, -CH-). ^{19}F NMR (CD_2Cl_2, δ ppm) : 76.86. FT-IR (cm^{-1}) : 3126 cm^{-1} (υCsp^2 / Csp^3 – H), 1600 cm^{-1} (υC=O), 1480 cm^{-1}. ESI (m/z) : $[M + H]^+$ = 217.04. UV-vis (absolute ethanol) : $\lambda_1$max = 327 nm. Band gap = 3.79 eV.

General Procedure for the Synthesis of the Complexes 1-5

 doi:10.20944/preprints202509.2570.v1

The synthesis (via Brønsted acid-base reaction), characterizations and purification of the non-hydrated complex **1** was performed under argon, starting from ligand **L^1H** (Scheme 1, left). The same reaction but treated under air led to the hydrated counterpart **2** (Scheme 1, right). Heteroleptic zinc complexes **3**-**5** were produced when nitrogen chelating Lewis base (LB) ligands such as TMEDA, bipy or *o*-phen) were added to the medium in a respective molar ratio Zn:LB of 1:1.

$[Zn(L^1)_2]_m$ (1)

Under argon, 1 g of 4,4,4-trifluoro-1-phenylbutane-1,3-dione **(L^1H)** (4.62 mmol) was vigorously stirred and dissolved in anhydrous hexane (20 mL). 3 mL of toluene solution of $ZnEt_2$ (2.31 mmol) were added dropwise at room temperature and the mixture was stirred overnight. The solvent was removed under vacuum and the resulting white solid was washed with anhydrous hexane and dried under vacuum to give 1 g of **1** (yield = 73 %). **1** was then stored in a glove box. The complex is soluble in polar solvents like acetone, tetrahydrofuran, acetonitrile and slightly soluble in dichloromethane, chloroform.

1 : $C_{20}H_{12}O_4F_6Zn$. MW = 495 g.mol^{-1}. ^{1}H NMR ($CDCl_3$, δ ppm) : 7.99 (4H, d, J = 7.43 Hz, HC_{ar}) ; 7.6 (2H, t, J = 7.36 Hz, HC_{ar}) ; 7.48 (4H, t, J = 7.36 Hz, HC_{ar}) ; 6.63 (2H, s, -CH-). ^{19}F NMR ($CDCl_3$, δ ppm) : -75.55.

$[Zn(L^1)_2(H_2O)_2]$ (2)

The same procedure used for the synthesis of compound **1** was repeated, except the reaction mixture was exposed to air immediately after the reaction was stopped. After solvent removal via rotary evaporation, a resulting white solid of **2** (2.2 g, 90 %) was obtained and collected by filtration after being washed by hexane. The complex is soluble in polar solvents such as acetone, tetrahydrofuran, acetonitrile, and slightly soluble in dichloromethane and chloroform. Colourless single crystals suitable for X-ray diffraction were obtained by slow evaporation from an acetonitrile solution of **2**.

2 : $C_{20}H_{16}O_6F_6Zn$. MW = 531 g.mol^{-1} ^{1}H NMR ($CDCl_3$, δ ppm) : 7.92 (4H, d, J = 8.16 Hz, HC_{ar}) ; 7.6 (2H, t, J = 7.05 Hz, HC_{ar}) ; 7.48 (4H, t, J = 7.92 Hz, HC_{ar}) ; 6.6 (2H, s, -CH-). ^{19}F NMR ($CDCl_3$, δ ppm) : -75.58 ppm. FT-IR (cm^{-1}) : 3363 cm^{-1} (υO–H of H_2O), 3070 cm^{-1} (υCsp^2 – H), 1606 cm^{-1} (υC=O), 1573 cm^{-1} (υC=C), 1311 cm^{-1} (υC–O). ESI (m/z) : $[M + Na^+]^+$ = 516.98. UV-vis (Absolute ethanol) : $\lambda_1$max = 328 nm. Band gap = 3.78 eV.

$[Zn(L^1)_2(TMEDA)]$ (3)

531 mg of $[Zn(L^1)_2(H_2O)_2]$ **2** (1 mmol) and 0.18 mL of TMEDA (1.2 mmol) were mixed in 10 mL of THF and the mixture stirred for 18 hrs at room temperature. Both THF and TMEDA were removed by rotary evaporator at 65 °C. The resulting white solid **3** (0.46 g, 80 %) was washed with hexane (20 mL) and collected and dried on a Büchner. The complex is moderately soluble in highly polar solvents such as acetone and acetonitrile but only slightly soluble in less polar solvents such as dichloromethane, chloroform and others. Colorless single crystals suitable for X-ray diffraction were obtained by slow evaporation from a saturated acetonitrile solution of **3.**

3 : $C_{26}H_{28}O_4F_6N_2Zn$. MW = 611 g.mol^{-1}. ^{1}H NMR ($(CD_3)_2CO$, δ ppm) : 7.91 (4H, d, J = 7.21 Hz, HC_{ar}) ; 7.50 (2H, t, J = 7.2 Hz, HC_{ar}) ; 7.39 (4H, t, J = 7.52 Hz, HC_{ar}) ; 6.28 (2H, s, -CH-) ; 2.85 (4H, s, -CH_2N) ; 2.49 (12H, s, CH_3N).^{19}F NMR ($(CD_3)_2CO$, δ ppm) : 100.89 ppm. FT-IR (cm^{-1}) : 2800-3070 cm^{-1} (υCsp^2 / Csp^3– H),1621 cm^{-1} (υC=O), 1573 cm^{-1} (υC=C), 1311 cm^{-1} (υC–O). ESI (m/z) : ESI (m/z) : $[M + Na^+]^+$ = 633.11. UV-vis (absolute ethanol) : $\lambda_1$max = 323 nm. Band gap = 3.84 eV.

$[Zn(L^1)_2(bipy)]$ (4)

The same procedure used for the synthesis of compound **3** was followed to give **4** by mixing 531 mg of **2** (1 mmol) and 187.5 mg of bipyridine (1.2 mmol) in 10 mL THF. After stirring, the resulting white solid **4** (0.334 g, 50 %) was obtained and washed with an ethyl acetate-hexane mixture (2:8) to

 doi:10.20944/preprints202509.2570.v1

remove the excess of bipyridine. The complex is soluble in polar solvents like acetone, tetrahydrofuran, acetonitrile and slightly soluble in dichloromethane and chloroform. Colorless single crystals suitable for X-ray diffraction were obtained by slow evaporation from a saturated acetonitrile solution of **4**.

4 : $C_{30}H_{20}O_4F_6N_2Zn$. MW = 651 g.mol^{-1} ^{1}H NMR ($(CD_3)_2CO$, δ ppm) : 8.82 (2H, d, J = 4.36 Hz, HC_{bipy}) ; 8.67 (2H, d, J = 8.24 Hz, HC_{bipy}) ; 8.33 (2H, td, ^{3}J = 1.4 Hz, ^{4}J = 9.07 Hz, HC_{bipy}) ; 7.85 (6H, m, HC_{bipy} + HC_{ar}) ; 7.5 (2H, t, J = 7.34 Hz, HC_{ar}) ; 7.39 (4H, t, J = 7.5 Hz, HC_{ar}) ; 6.33 (2H, s, -CH-). ^{19}F NMR ($(CD_3)_2CO$, δ ppm) : 101.19 ppm. FT-IR (cm^{-1}) : 3029-3114 cm^{-1} (υCsp^2 / Csp^3– H), 1612 cm^{-1} (υC=O), 1577 cm^{-1} (υC=C), 1311 cm^{-1} (υC–O). ESI (m/z) : $[M + Na^+]^+$ = 673.05. UV-vis (absolute ethanol) : λ$_1$max = 324 nm. Band gap = 3.83 eV.

$[Zn(L^1)_2(o\text{-}phen)]$ (5)

The same procedure used for the synthesis of compound **4** was followed for **5** by mixing 531 mg of **2** (1 mmol) and 218 mg of 1,10-phenanthroline.H_2O (1.1 mmol) in 10 mL THF. **5** (0.50 g, 74 %) was collected after its impure form **5** was dissolved in CH_3CN (50 mL : 10 mL for each 100 mg of product) in order to remove the excess of 1,10-phenanthroline which precipitated. This is followed by washing with hexane (20 mL) and drying on a Büchner to obtain the pure complex. The complex is soluble in polar solvents like acetone, tetrahydrofuran, acetonitrile and slightly soluble in dichloromethane and chloroform. Colourless single crystals suitable for X-ray diffraction were obtained by slow evaporation from a saturated acetonitrile solution of **5**.

5 : $C_{32}H_{20}O_4F_6N_2Zn$. MW = 675 g.mol^{-1}. ^{1}H NMR ($(CD_3)_2CO$, δ ppm) : 9.13 (2H, dd, J = 4.16 Hz and J = 1.31 Hz, $HC_{o\text{-}phen}$) ; 8.86 (2H, dd, J = 8.33 Hz and J = 1.34 Hz, $HC_{o\text{-}phen}$) ; 8.23 (2H, dd, J = 8.22 Hz and J = 4.3 Hz, $HC_{o\text{-}phen}$) ; 8.14 (2H, q, J = 8.2 Hz, $HC_{o\text{-}phen}$) ; 7.89 (4H, d, J = 7.22 Hz, HC_{ar}) ; 7.49 (2H, t, J = 7.3 Hz, HC_{ar}) ; 7.4 (4H, t, J = 7.44 Hz, HC_{ar}) ; 6.4 (2H, s, -CH-). ^{19}F NMR ($(CD_3)_2CO$, δ ppm) : 101.27 ppm. FT-IR (cm^{-1}) 3025-3070 cm^{-1} (υCsp^2 / Csp^3– H), 1610 cm^{-1} (υC=O), 1575 cm^{-1} (υC=C), 1286 cm^{-1} (υC–O). ESI (m/z) : $[M + Na^+]^+$ = 697.05. UV-vis (absolute ethanol) : λ$_1$max = 322 nm. Band gap = 3.85 eV.

5. Conclusions

This work establishes the synthesis and characterization of a new series of homoleptic and heteroleptic Zn(II) β-diketonate complexes. The structural, thermal, and photophysical data collectively reveal how molecular design dictates material properties. Single-crystal X-ray diffraction confirmed monomeric octahedral geometries, where ancillary nitrogen-based ligands introduce specific distortions. Thermogravimetric analysis demonstrated enhanced thermal stability, supporting their viability as precursors. The most significant outcome stems from ultrafast spectroscopic studies, which showed that coordination to zinc fundamentally redirects the photophysical pathway of the β-diketonate ligand. Unlike the free ligand, which relaxes rapidly to the ground state, the zinc-complexed form populates a long-lived triplet state. This capacity to generate a persistent, chemically reactive species upon photoexcitation is the critical feature that makes these complexes compelling candidates for applications in laser-induced deposition and the fabrication of 3D ZnO nanostructures. Consequently, this study establishes a rational framework for designing functional precursors with tailored excited-state properties for advanced photonic and electronic applications.

Supplementary Materials: The following supporting information can be downloaded at the website of this paper posted on Preprints.org. **Spectroscopic Characterizations:** Complex **1**: NMR ($CDCl_3$, 300 MHz, ^{1}H and ^{19}F); Complex **2**: NMR ($CDCl_3$, 300 MHz, ^{1}H and ^{19}F); Complex **3**: NMR ($(CD_3)_2CO$, 300 MHz, ^{1}H and ^{19}F); Complex **4**: NMR ($(CD_3)_2CO$, 300 MHz, ^{1}H and ^{19}F); Complex **5**: NMR ($(CD_3)_2CO$, 300 MHz, ^{1}H and ^{19}F). **Single-Crystal X-ray Characterizations of the zinc complexes**: Complex **2**; Complex **3**; Complex **4**; Complex **5**. **Infrared spectra**: **Figure S1:** Infrared spectrum of ligand **L^1H**; **Figure S2:** Infrared spectrum of complex **2**; **Figure S3:** Infrared spectrum of complex **3**; **Figure S4:** Infrared spectrum of complex **4**; **Figure S5:** Infrared spectrum of complex **5**. **UV–Vis absorption spectroscopy**: **Figure S6:** The UV–Vis study of the ligand **L^1H** and its

 doi:10.20944/preprints202509.2570.v1

corresponding complexes (**2–5**). **Thermal Analysis:** The thermal property (TGA) study of the ligand **L¹H** and its corresponding complexes (**1–5**). **ESI/FAB Mass Spectrometry**: **Figure S8:** Mass spectrometry of **complex 2**; **Figure S9:** Mass spectrometry of **complex 3**; **Figure S10:** Mass spectrometry of **complex 4**; **Figure S11:** Mass spectrometry of **complex 5**. **Femtosecond transient absorption spectroscopy (TAS): Figure S12**: Transient absorption spectra of complex [Zn(L^1)$_2$(TMEDA)] **(3)** recorded in ethanol with a pump excitation λ_{pump} = 320 nm; Transient absorption spectra of compounds [Zn(L^1)$_2$(bipy)] (**4**) recorded in ethanol with a pump excitation λ_{pump} = 320 nm; Transient absorption spectra of compounds [Zn(L^1)$_2$(*o*-phen)] (**5**) recorded in ethanol with a pump excitation λ_{pump} = 320 nm. Crystal data were deposited in the CCDC with the numbers 2384613, 2384615**,** 2384616, 2384614**,** for the complexes **2**, **3**, **4**, **5**.

Author Contributions: Conceptualization, S.D; methodology, A.D.;V.D.W. and S.D.; formal analysis, A.D.; M.C.; T.R.; V.D.W. and S.D.; investigation, A.D. and M.C.; writing—original draft preparation, A.D.; V.D.W. and S.D.; writing—review and editing, A.D.; V.D.W. and S.D.; supervision, T.R.; V.D.W. and S.D.; project administration, V.D.W. and S.D.; funding acquisition, V.D.W. and S.D. All authors have read and agreed to the published version of the manuscript

Funding: This work was funded by the Agence Nationale de la Recherche (ANR) [grant number ANR-23-CE08-0010-02] trough the project "ACTIVATE". fs-TAS measurements have been carried using the ultrafast spectroscopy facility of the Advanced Characterization Platform of the Chevreul Institute. This work is part of the ULTRAFAST/OPERANDO of PEPR LUMA platform, France 2030 Funding (ANR-22-EXLU-0002/ANR-22-EXLU-000).

Acknowledgments: The authors acknowledge access to the facilities at the IEMN and thank Prof. François Courvoisier and Prof. Ausrine Bartasyte (FEMTO-ST) for fruitful discussions.

Conflicts of Interest: The authors declare no conflicts of interest.

Abbreviations

The following abbreviations are used in this manuscript:

FT-IR Fourier Transform Infrared Spectroscopy
ESI/FAB Electrospray Ionization / Fast Atom Bombardment Mass Spectrometry
UV–Vis Ultraviolet–Visible Spectroscopy
TGA Thermogravimetric Analysis
ZnO Zinc Oxide
TMEDA N,N,N′,N′-Tetramethylethylenediamine
bipy 2,2′-Bipyridine
o-phen 1,10-Phenanthroline
CIF Crystallographic Information File
LMCT Ligand-to-Metal Charge Transfer
ESA Excited State Absorption

References

1. Stienen, C.; Grahl, J.; Wolper, C.; Schulz, S.; Bendt, G. Fluorinated β-diketonate complexes M(tfac)$_2$(TMEDA) (M = Fe, Ni, Cu, Zn) as precursors for the MOCVD growth of metal and metal oxide thin films. *RSC Adv.* **2022**, *12*, 22974–22983
2. Bijou, D.; Cornier, T.; Mishra, S.; Merzoud, L.; Chermette, H.; Jeanneau, E.; Maudez, W.; Benvenuti, G.; Daniele, S. Synthesis and Thermal Behavior of Heteroleptic γ-Substituted Acetylacetonate-Alkoxides of Titanium. *Eur. J. Inorg. Chem.* **2021**, *20*, 1976–1983
3. Cao, Y.; Xu, D.; Yang, M.; Wang, Y.; Zhou, F.; Zhou, H. β-Diketonate ligands for photophysical applications. *Asian J. Chem.* **2013**, *25*, 6900
4. Wang, Y.; Xiong, W.; Zhang, X.; et al. Glycerol-assisted grain modulation in femtosecond-laser-induced photochemical synthesis of patterned ZnO nanomaterials. *Light: Adv. Manuf.* **2025**, *6*, 7

5. Lee, H. S.; An, S.; Kim, Y.; Kim, D. K.; Kang, J. K.; Choi, Y. W.; Lee, S. G.; O, B. H.; Lee, E. H. Microfabrication of 3D microstructures using ZnO precursors. *Microelectron. Eng.* **2006**, *83*, 1347–1351
6. Zhao, H.; Zhou, X.; Yu, J.; Mummery, P. Advances in micro/nano fabrication for functional materials. *Fusion Eng. Des.* **2013**, *88*, 2453–2456.
7. Wibowo, A.; Marsudi, M. A.; Amal, M. I.; Ananda, M. B.; Stephanie, R.; Ardy, H.; Diguna, L. J. Organic–inorganic hybrid microstructures for additive manufacturing. *RSC Adv.* **2020**, *10*, 42838–42859
8. Ramelan, A. H.; Wahyuningsih, S.; Munawaroh, H.; Narayan, R. Fabrication of micro/nano devices using multiphoton precursors. *IOP Conf. Ser.: Mater. Sci. Eng.* **2017**, *176*, 012008
9. Cho, H.; Strader, M. L.; Hong, K.; Jamula, L.; Gullikson, E. M.; Kim, T. K.; de Groot, F. M. F.; McCusker, J. K.; Schoenlein, R. W.; Huse, N. Ultrafast spectroscopy of metal–ligand complexes. *Faraday Discuss.* **2012**, *157*, 463;
10. Hervé, M.; Boyer, A.; Brédy, R.; Compagnon, I.; Lépine, F. Advances in ultrafast photophysics. *Adv. Phys. X* **2022**, *7*, 2123283
11. Wang, H.; Bokarev, S. I.; Aziz, S. G.; Kühn, O. Femtosecond dynamics in metal–organic complexes. *Phys. Rev. Lett.* **2017**, *118*, 023001
12. Banerjee, A.; Coates, M. R.; Kowalewski, M.; Wikmark, H.; Jay, R. M.; Wernet, P.; Odelius, M. Time-resolved studies of ligand-to-metal charge transfer. *Nat. Commun.* **2022**, *13*, 1337
13. Salassa, L.; Garino, C.; Salassa, G.; Gobetto, R.; Nervi, C. Structural analysis of Zn β-diketonates. *J. Am. Chem. Soc.* **2008**, *130*, 9590
14. Záliš, S.; Busby, M.; Kotrba, T.; Matousek, P.; Towrie, M.; Vlček, A. Coordination geometries of heteroleptic complexes. *Inorg. Chem.* **2004**, *43*, 1723
15. Zakrzewski, J.; Delaire, J. A.; Daniel, C.; Cote-Bruand, I. Structural versatility of metal–β-diketonates. *New J. Chem.* **2004**, *28*, 1514
16. Shi, P.; Jiang, Q.; Zhao, X.; Zhang, Q.; Tian, Y. Femtosecond laser deposition of ZnO. *Dalton Trans.* **2015**, *44*, 8041
17. Yang, L.; Hu, H.; Scholz, A.; Feist, F.; Cadilha Marques, G.; Kraus, S.; Bojanowski, N. M.; Blasco, E.; Barner-Kowollik, C.; Aghassi-Hagmann, J.; Wegener, M. Micro/nano printing of 3D ZnO structures. *Nat. Commun.* **2023**, *14*, 1103
18. Hemaa, M. K.; Karthik, C. S.; Mahesha; Pampa, K. J.; Mallu, P.; Lokanath, N. K. 4,4,4-Trifluoro-1-phenylbutane-1,3-dione metal [Cu(II) and Ni(II)] complexes as a superlative antibacterial agent against MRSA: Synthesis, structural quantum-chemical and molecular docking studies. *J. Mol. Struct.* **2021**, *1243*, 130774
19. Grassie, N. Polymer Degradation and Char Formation. In *The Chemistry and Technology of Polymer Degradation and Stabilization*; Elsevier: London, **1995**, 45–67
20. Verma, P.; Koch, F.; Steinbacher, A.; Nuernberger, P.; Brixner, T. Ultrafast UV-Induced Photoisomerization of Intramolecularly H-Bonded Symmetric β-Diketones. *J. Am. Chem. Soc.* **2014**, *136*, 14981–14989.
21. Wang, J.; Lei, Y.; Guo, Y.; Wang, J.; Ma, J. Investigation of Different Photochemical Reactions of Avobenzone Derivatives by Ultrafast Transient Absorption Spectroscopy. *Photochem. Photobiol. Sci.* **2019**, *18*, 3000–3007
22. Perrinet, Q.; Ghosh, A. C.; Canivet, J.; Wisser, F.; Roland, T.; De Waele, V. Unexpected Interference of the Triethanolamine Sacrificial Electron Donor with the Excited States of Molecular and Heterogenized Rhodium Bipyridine Photocatalysts Revealed by Femtosecond Transient Absorption Spectroscopy. *J. Phys. Chem. C* **2025**, *129*, 1313–1326